Journal of Controlled Release 174 (2014) 15–26

Contents lists available at ScienceDirect

Journal of Controlled Release

journal homepage: www.elsevier.com/locate/jconrel

Polymeric nanoparticle system to target activated microglia/macrophages in spinal cord injury

Simonetta Papa [a,1], Raffaele Ferrari [b,1], Massimiliano De Paola [c], Filippo Rossi [b], Alessandro Mariani [c], Ilaria Caron [a], Eliana Sammali [a], Marco Peviani [d], Valentina Dell'Oro [a], Claudio Colombo [b], Massimo Morbidelli [g], Gianluigi Forloni [a], Giuseppe Perale [b,e,f], Davide Moscatelli [b], Pietro Veglianese [a,*]

[a] IRCCS Istituto di Ricerche Farmacologiche "Mario Negri", Dipartimento di Neuroscienze, via La Masa 19, 20156 Milan, Italy
[b] Politecnico di Milano, Dipartimento di Chimica, Materiali e Ingegneria Chimica "Giulio Natta", via Mancinelli 7, 20131 Milan, Italy
[c] IRCCS Istituto di Ricerche Farmacologiche "Mario Negri", Dipartimento di Ambiente e Salute, via La Masa 19, 20156 Milan, Italy
[d] Università di Pavia, Dipartimento di Biologia e Biotecnologie "L. Spallanzani", via Ferrata, 9, 27100 Pavia, Italy
[e] Department of Innovative Technologies, University of Applied Sciences and Arts of Southern Switzerland, SUPSI, via Cantonale, CH-6928 Manno, Switzerland
[f] Swiss Institute for Regenerative Medicine, CH-6807 Taverne, Switzerland
[g] Institute for Chemical and Bioengineering, ETH Zurich, Campus Hoenggerberg, HCI F125, Wolfgang Pauli Str. 10, 8093 Zurich, Switzerland

ARTICLE INFO

Article history:
Received 25 July 2013
Accepted 1 November 2013
Available online 10 November 2013

Keywords:
Nanoparticle
Microglia
Macrophage
Spinal cord injury
Drug delivery

ABSTRACT

The possibility to control the fate of the cells responsible for secondary mechanisms following spinal cord injury (SCI) is one of the most relevant challenges to reduce the post traumatic degeneration of the spinal cord. In particular, microglia/macrophages associated inflammation appears to be a self-propelling mechanism which leads to progressive neurodegeneration and development of persisting pain state. In this study we analyzed the interactions between poly(methyl methacrylate) nanoparticles (PMMA-NPs) and microglia/macrophages *in vitro* and *in vivo*, characterizing the features that influence their internalization and ability to deliver drugs. The uptake mechanisms of PMMA-NPs were in-depth investigated, together with their possible toxic effects on microglia/macrophages. In addition, the possibility to deliver a mimetic drug within microglia/macrophages was characterized *in vitro* and *in vivo*. Drug-loaded polymeric NPs resulted to be a promising tool for the selective administration of pharmacological compounds in activated microglia/macrophages and thus potentially able to counteract relevant secondary inflammatory events in SCI.

1. Introduction

"Secondary injury" is considered the main cause of the post traumatic neural degeneration in SCI [1–3]. It is characterized by a wide spectrum of events that allows to classify SCI as a multi-factorial disease [4,5]. It is now well understood that the most important aim for neuroprotection of the traumatized cord is to counteract the mechanisms of this secondary injury and to minimize their pathological consequences [4,6]. A growing number of potential therapeutic interventions in SCI repair are focused on this target, but unfortunately none of them had shown relevant therapeutic effects when translated to humans [4,6,7]. Recent discoveries demonstrated that acute and chronic inflammation, represented by microglia and cellular infiltration (neutrophils, macrophages and lymphocytes), which subsequently induced the release of inflammatory mediators (cytokine and chemokines), is tightly involved in the progression of the spinal cord degeneration [8,9]. Among the cells recruited in the inflammatory events, a key role is played by microglia/macrophages [10,11]. Microglia are able to rapidly respond to insults, changing their own phenotype toward an amoeboid or phagocytic activated shape. Recently a dual role (harmful or beneficial) has been associated with different activated microglia phenotypes (M1 and M2) during the progression of the traumatic event [12,13]. M1 phenotype, which is associated with a detrimental effect, shows an early- and long-term activation up to the chronic phase of SCI, whereas, M2 phenotype, characterized by a protective effect, shows a transient expression only in a subacute phase [12]. This suggests that microglia/macrophages associated inflammation could be a persistent deleterious event during the chronicity phase of the neurodegeneration, representing a crucial therapeutic target for SCI treatment [14,15]. On the basis of that, a promising strategy to counteract the propagation of the secondary injury associated to the inflammatory response in SCI might be the selective pharmacological targeting of activated microglia/macrophages.

Recent advances in polymer science have provided many innovations, underlining an increasing importance of polymeric nanoparticles

* Corresponding author. Tel.: +39 0239014205; fax: +39 023546277.
E-mail address: pietro.veglianese@marionegri.it (P. Veglianese).
[1] Contributed equally to this work.

0168-3659/$ – see front matter © 2013 Elsevier B.V. All rights reserved.
http://dx.doi.org/10.1016/j.jconrel.2013.11.001

(NPs) as a promising drug delivery tool [16–18]. Indeed, thanks to their flexibility in terms of size, hydrophilic/lipophilic characteristics and surface functionalization, NPs offer relevant advantages in drug delivery by targeting molecules in specific cells and controlling drug release over time [16,18–21].

Much evidence has demonstrated that the intrinsic capacity of macrophages to internalize foreign bodies can be exploited for targeting drug delivery using NPs [22–25]. It is also well-known that microglial cells, when activated, carry out a macrophage-like phagocytic activity [10]. In this context, we investigated the potential use of poly(methyl methacrylate) NPs (PMMA-NPs) as a delivery tool to selectively target microglia/macrophages. Among the large number of polymer NPs reported in literature, PMMA-based NPs exhibit important characteristics such as extremely narrow size distribution and good mechanical stability. Such NPs do not show significant toxic effects since they do not alter main biological features such as viability, cell growth and metabolic activity, as recently demonstrated in both tumor and stem cells [26,27]. Moreover, PMMA-based NPs possess a great potential as drug delivery vector due to the possibility in producing pH- and thermo-responsive NPs and nanocomposites [28,29].

PMMA-NP uptake kinetics by activated microglia was studied *in vitro*, considering NPs with different features such as surface charge and PEGylation. Then, the possibility to adopt such NPs as drug carrier to target activated microglia/macrophages was investigated by evaluating the possibility to internalize and diffuse into microglia/macrophages cytosol a mimetic drug compound (To-Pro3) both *in vitro* and *in vivo*.

2. Materials and methods

2.1. Fluorescent PMMA-NP synthesis and characterization

Rhodamine B (RhB, Sb sensitivity < 0.1 μg mL^{-1}, Carlo Erba reagents), 2-hydroxyethyl methacrylate (HEMA; 97% purity, ABCR), dicyclohexylcarbodiimide (DCC; 99% purity, Sigma-Aldrich, Italy), 4-(dimethylamino)-pyridine (DMAP; >99% purity, Sigma-Aldrich, Italy), Acetonitrile (ACN, ≥99.9% purity, Sigma-Aldrich, Italy), methyl methacrylate (MMA, 99.5%, Sigma-Aldrich, Italy), 2-ethylhexanoic acid tin(II) salt ($Sn(Oct)_2$, ~95%, Sigma-Aldrich, Italy), potassium persulfate (KPS; >99% purity, ACS reagent), 2,2′-Azobis(2-methylpropionamidine) dihydrochloride (Sigma-Aldrich, Italy), poly(ethylene glycol) methyl ether methacrylate (HEMA-PEG_{19}, molecular weight: ca. 950 Da) (Sigma-Aldrich, Italy), and polyoxyethylenesorbitan monooleate (Tween80; Sigma-Aldrich, Italy) were used for NP synthesis as received. For HPLC analyses, acetonitrile, ammonium acetate, and methanol were used (Sigma-Aldrich, Italy).

2.2. Fluorescent macromonomer (HEMA-RhB) synthesis and characterization

The synthesis of the HEMA-RhB macromonomer was performed as follows [27]: the esterification between HEMA and RhB was promoted by DCC, as esterification agent, and DMAP, as catalyst. In particular, 1 g of RhB, dissolved in 20 mL of ACN and 0.325 g of HEMA were loaded together in a beaker and placed under magnetic stirring, 0.43 g of DCC and 13 mg of DMAP were dissolved in 20 mL of ACN and added dropwise in the RhB and HEMA solution. The addition was concluded in 20 min. The reaction was run for 24 h at 40 °C, kept constant using an oil bath, under magnetic stirring (350 rpm). Next, reaction media was quenched in ice bath for 10 min, leading to the complete dicyclohexylurea (DCU) precipitation. DCU coming from the DCC hydration was removed by filtration, DCU yield was measured gravimetrically as equal to 86%. Dried HEMA-RhB macromonomer was obtained by removing ACN using a Rotavapor.

The produced macromonomer, which indeed contains not reacted RhB, as proved by the yield of DCU lower than 100%, has been chromatographically purified adopting an Agilent 1100 Series HPLC, equipped with an auto-sampler, a diode array detector, an online-degasser and an isocratic pump (buffer used: 40% acetonitrile, 0.1% trifluoroacetic acid, column used: Kromasil 100-10C18 preparative column, dimensions: 250 × 4.6 mm). Fractions correspondent to the pure macromonomers were collected using a Gilson FC 203B fraction collector connected at the outlet of the HPLC.

2.3. Nanoparticle synthesis and characterization

PMMA-NPs were synthesized through free radical emulsion polymerization performed in batch conditions (batch emulsion polymerization, BEP) by using KPS or 2,2′-Azobis(2-methylpropionamidine) dihydrochloride as initiators, and Tween80 as surfactant [30]. Reaction was carried out using a 100 mL three necked glass flask equipped with a reflux condenser. Temperature was controlled with an external oil bath set to 80 ± 1 °C. Different mass of Tween80 was added to 50 mL of deionized water and the atmosphere of the reactor was kept inert through vacuum-nitrogen cycles. After that, for BEP reaction, 2.5 g of MMA, in which a proper amount of HEMA-RhB macromonomer was previously dissolved (0.1% $w_{HEMA\text{-}RhB}/w_{MMA}$), was injected in the purged system with a syringe. The system was maintained under magnetic stirring at 350 rpm. Finally, 0.04 g of the proper initiator was added to initiate the reaction. The reaction was run for 3 h; final monomer conversion has been measured through gravimetric measurement and calculated as higher than 99.5%. After the synthesis the pH was adjusted to 7 using NaOH 0.1 M. The final solid content of the latex was measured as 5% w/w. In particular, NPs were obtained using the following recipes:

- PMMA: 20% Tween80/MMA ratio, KPS as initiator in BEP.
- PMMA_pos: 5% Tween80/MMA ratio, 2,2′-Azobis(2-methyl propionamidine) dihydrochloride as initiator in BEP.

PEGylated PMMA-NPs were produced adopting a monomer starved semi-batch emulsion polymerization (MSSEP) [31]. This procedure consists in the loading of the hydrophilic macromonomer (HEMA-PEG_{19}) in the reactor as in a normal batch polymerization while the more hydrophobic monomer (MMA in this case) is injected as in a semi-batch process. All the experiment setup was the same as described above; in addition HEMA-PEG_{19} and Tween80 were previously loaded into the reactor while the solution of the two monomers (MMA and HEMA-RhB) was injected into the system with a flow rate of 3 mL/h using a syringe pump (Model NE-300, New Era Pump System, Farmingdale, US) after the initiator injection in the purged solution. The total amount of involved monomers was 2.5 g in order to ensure a final solid content of 5% w/w. In particular, PEGylated NPs were obtained using the following recipes:

- PMMA_PEG: 15% Tween80/Monomer ratio, 0.5 g HEMA-PEG_{19}, 2 g of MMA, KPS as initiator in MSSEP.

The size and polydispersity index of the NP suspension were collected from Dynamic Light Scattering (DLS) measurements (Malvern, Zeta Nano ZS), and the reported data are an average value of two measurements of the same sample.

The size and morphology of the produced NPs were confirmed through morphological analysis carried out by transmission electron microscopy (TEM) by using Philips CM200-FEG transmission electron microscope working at 2000 kV. Samples were prepared placing a 5 μL drop of NP colloidal suspension on a Formvar/carbon-coated copper grid and dried overnight. Digital images were acquired by a charge coupled device (CCD) Esi Vision Proscan camera.

2.4. NP stability in cell medium

The NP stability has been verified maintaining the NPs for 72 h at 37 °C in the same medium used for the cellular growth. The measured

Table 1
Characteristics of the produced PMMA-NP nanoparticles.

Sample		Post synthesis					72 h incubation with cell medium	
		Size	D50	D90	Polydispersity index	ζ potential	Size	Polydispersity index
		[nm]	[nm]	[nm]	[–]	[mV]	[nm]	[–]
1	PMMA	92	91	142	0.082	−18.0	104	0.101
2	PMMA_pos	97	98	164	0.065	21.5	106	0.110
3	PMMA_PEG	90	88	122	0.090	−2.52	94	0.098

average particle size, reported in Table 1, does not show any significant changes in terms of both size and polydispersity index, meaning that no aggregation took place and, consequently, that the NPs are stable in the selected medium as also detectable from the particle size distribution reported in Fig. 1A.

2.5. NP loading with To-Pro3 and in vitro delivery

To-Pro3 (Invitrogen, Italy) was loaded in NPs after the polymerization reaction. Firstly, PMMA-NP latex concentration was increased under vacuum at room temperature with the use of a Rotavapor apparatus (Buchi instruments). 1 ml of PMMA-NP latex at 25% w/w was obtained with the absence of aggregates as confirmed by DLS measurements. The concentrated latex was incubated with 20 μg To-Pro3 for one day at room temperature under gentle magnetic stirring. Latex was then diluted to the desired concentration (2.5% w/w). Loading efficiency (% loading) was calculated based on the following equation:

$$\%\ \text{loading} = \frac{\text{To-Pro3 entrapped in NPs}}{\text{Initial amount of To-Pro3 added}} \cdot 100. \quad (1)$$

NPs, loaded with To-Pro3, at concentration of 1% wt/wt were placed in excess of phosphate buffered saline solution (PBS) at 37 °C and aliquots were collected at defined time points, while the sample volume was replaced by fresh PBS, in order to avoid mass-transfer equilibrium with the surrounding solution. The supernatant of the NPs was recovered using Vivaspin 500 (Sartorius Stedim, UK). The aliquot was added to the Vivaspin 500 and the system was centrifuged at 4000 rpm for 15 min. Then, the following procedure was repeated two times to ensure a complete supernatant recovery: 100 μL of deionized water was added to the

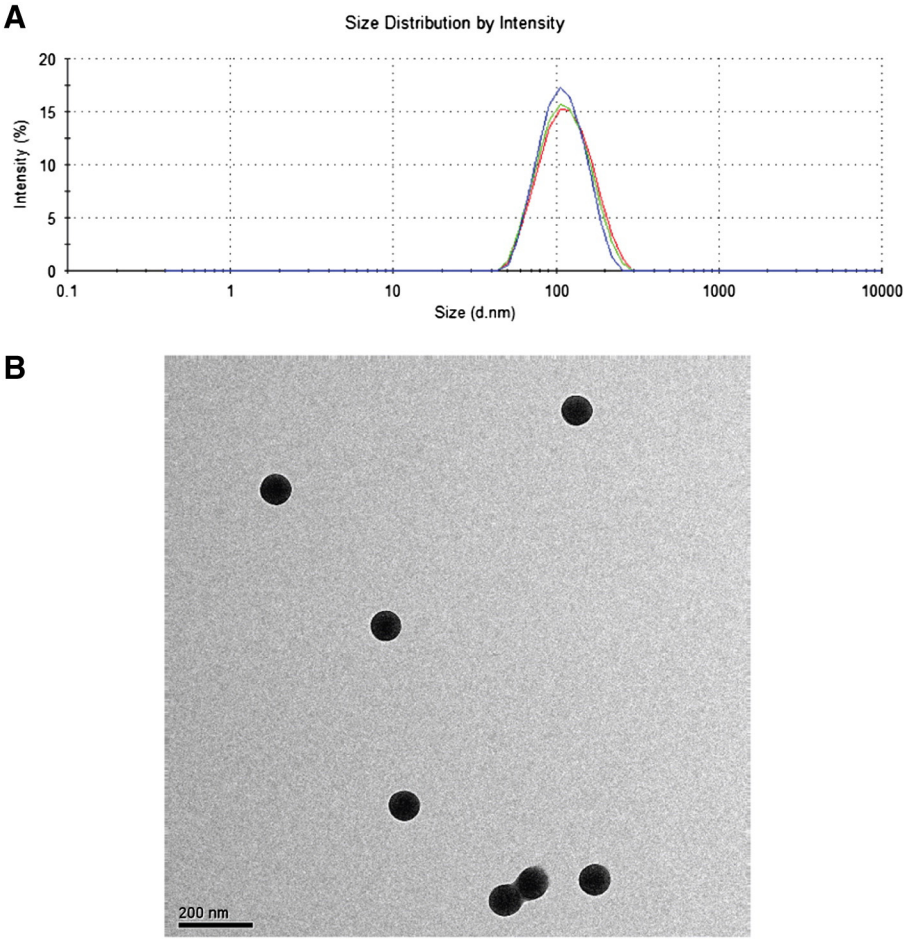

Fig. 1. (A) Intensity particle size distribution of PMMA (blue line), PMMA_pos (red line), and PMMA_PEG (blue line). (B) TEM of PMMA-NPs. (For interpretation of the references to color in this figure legend, the reader is referred to the web version of this article.)

Vivaspin and the system was centrifuged at 4000 rpm for 15 min. Percentage of To-Pro3 released was measured by spectroscopy. Results were expressed as average percentage released ± standard deviation, n = 3.

2.6. Animals and their care

Procedures involving animals and their care were conducted in conformity with the institutional guidelines at the IRCCS — Institute for Pharmacological Research "Mario Negri" in compliance with national (Decreto Legge nr 116/92, Gazzetta Ufficiale, supplement 40, February 18, 1992; Circolare nr 8, Gazzetta Ufficiale, July 14, 1994) and international laws and policies (EEC Council Directive 86/609, OJL 358, 1, Dec. 12, 1987; Guide for the Care and Use of Laboratory Animals, US National Research Council (eighth edition) 2011).

2.7. Primary cell cultures

Primary cultures of microglia or neuron/glia co-cultures were obtained from the spinal cord of 13-day-old C57 BL/6J mouse embryos as previously described [32]. Briefly, spinal cords were dissected, exposed to DNAse and trypsin (Sigma-Aldrich, Italy) and centrifuged through a BSA cushion. Cells obtained at this step were a mixed neuron/glia population and underwent centrifugation through a 6% iodixanol (OptiPrep™, Sigma-Aldrich, Italy) cushion to separate large neurons from glial cells. The glial feeder layer was prepared by plating the glial fraction at a density of 25,000 cells/cm^2 into 12-well plates or into flasks, both previously precoated with poly-L-lysine (Sigma-Aldrich, Italy). Purified microglia were obtained from flasks containing confluent mixed glial cultures after overnight shaking at 275 rpm in incubators. The supernatants (containing microglia) were collected and seeded at a density of 20,000 cells/cm^2. Astrocyte cultures were obtained by treating the glial cultures, from which microglia had been previously harvested, with 60 mM L-leucine methyl ester (Sigma-Aldrich, Italy) for 90 min. To establish neuron/glia co-cultures, the neuron-enriched fraction (obtained from the iodixanol-based separation) was seeded at a density of 10,000 cells/cm^2 onto a mature astrocyte layer and microglia were added (10% of the astrocyte number) on the third day *in vitro*.

2.8. Culture treatments

Microglia activation was induced by exposing purified microglia cultures or neuron/glia co-cultures to 1 μg/mL LPS (from *Escherichia coli* 0111:B4; Sigma-Aldrich, Italy) for 18 h, as previously reported in De Paola et al. [33]. Cultures maintained with normal medium served as the control condition. PMMA-NPs (0.05% weight/volume) were then added to untreated or LPS-stimulated cultures. For the chlorpromazine hydrochloride (CPZ; Sigma-Aldrich, Italy) treatments, different solutions of CPZ (final concentrations: 30, 40 or 50 μM) were added to the culture medium 2 h before PMMA-NP exposure.

2.9. Cell viability assay

The CellTiter^{96}® AQueous Non-Radioactive Cell Proliferation Assay (MTS; Promega, Italy) and propidium iodide (1 μg/ml, AbD Serotec, Italy) were used accordingly to the manufacturer's instruction to determine cell viability in PMMA-NP treated microglial cells.

2.10. Immunocytochemistry

Cells were fixed with 4% paraformaldehyde and, when indicated, permeabilized by 0.2% Triton X-100 (Sigma-Aldrich, Italy). Staining was carried out by overnight incubation with primary antibodies, followed by incubation with an appropriate fluorescent secondary antibody. Cell nuclei were labeled with Hoechst 33258 (250 ng/mL, Invitrogen, Italy). Double or triple stainings were carried out by overnight incubation of the cultures separately with each primary antibody. In each experiment, some wells were processed without the primary antibody to verify the specificity of the staining. The following primary antibodies were used: anti-neurofilament 200 (rabbit, 1:500; Sigma-Aldrich, Italy); anti-GFAP (rabbit, 1:500; Millipore, Italy) and anti-CD11b (rat, 1:1000; eBioscience Inc., Italy). Appropriate fluorescent secondary antibodies (Dy-light; Rockland Immunochemicals Inc., Italy) conjugated to different fluorochromes were used (1:1.000).

2.11. Quantitative enzyme-linked immunosorbent assays (ELISA)

After LPS stimulation of microglia for 18 h, the culture medium was removed and PMMA-NPs were added for additional 24 h. Then, TNFα, IL-6 and IL-1β concentrations in cell culture supernatants were quantified by solid-phase sandwich ELISA (eBioscience Inc.). Samples from each experiment were tested in triplicate, accordingly to the manufacturer's instructions.

2.12. Hydrogel synthesis

Hydrogels (Agarose Carbomer, AC) were prepared by copolymerization in PBS at about 80 °C, where polymeric solution (carbomer 974P 0.5 wt.%, agarose 0.1 wt.%) was achieved by mixing polymer powders into the selected solvent, adding a mixture of cross-linking agents primarily made of propylene glycol (30 wt.%) and glycerol (1.2 wt.%) (along with NaOH 1 N 3 wt.% for pH neutralization). Reaction pH was indeed kept neutral. Polycondensation was achieved by microwave heating for 1 min per 10 mL of polymeric solution [34], after synthesis reaction hydrogel was mixed with NPs (1% monomer concentration), while gelation occurred *in situ* after injection [35].

2.13. Surgery

Hydrogel injection: Before surgery, the mice (female, weight = 30 g) received an antibiotic and analgesic treatment, respectively with a subcutaneous injection of ampicillin (50 mg/kg) and buprenorphine (0.15 mg/kg). The entire surgical procedure was carried out in deep anesthesia by Ketamine hydrochloride (Imalgene, 100 mg/kg, Alcyon Italia S.p.A.) and medetomidine hydrochloride (Domitor, 1 mg/kg, Alcyon Italia S.p.A.) intraperitoneally injected. T11 and T12 vertebrae were identified and exposed by separation of dorsal and intervertebral muscles. Animals were then placed on a Cunningham Spinal Cord Adaptor (Stoelting, Dublin, Ireland) mounted on a stereotaxic frame, laminectomy of T12 vertebra was done to uncover the lumbar spinal cord and dura mater was cut and reflected. Using a glass capillary (40 ± 2 μm diameter) the hydrogel AC/PMMA-NP solution (0.5 μL/site) was injected in the spinal cord with a flow rate of 0.2 μL/min. Stereotaxic coordinates were referred to the midline of the dorsal horn of the spinal cord. The capillary was positioned at +0.5 mm aside from the midline, then it was deepened into the parenchyma to 0.7 mm below the pia mater. The injector was left in place for 1 min and then retracted for 0.2 mm before starting the delivery. After gel injection, the capillary was left in place for additional 3 min and then gently withdrawn.

2.14. Hydrogel positioning

Thirty-nine mice were enrolled for the surgery and randomly divided into 3 groups of 13 animals each (female, weight = 30 g): healthy animals (CTR), injured animals (SCI) and injured animals treated with PMMA-NPs (SCI + PMMA). Before the surgery the animals received an antibiotic and analgesic treatment, respectively with a subcutaneous injection of ampicillin (50 mg/kg) and buprenorphine (0.15 mg/kg). The entire surgical procedure was carried out in deep anesthesia by ketamine hydrochloride (Imalgene, 100 mg/kg, Alcyon Italia S.p.A.) and medetomidine hydrochloride (Domitor, 1 mg/kg, Alcyon Italia S.p.A.)

intraperitoneally. The back of the animal was shaved at dorsal level and a cutaneous incision (3 cm) was performed to expose the backbone. T11 and T12 vertebrae were identified and exposed by separation of dorsal and intervertebral muscles. The animals were then placed in a Cunningham Spinal Cord Adaptor (Stoelting, Ireland) mounted on a stereotaxic frame, and laminectomy of the T11 vertebra was done to uncover thoracic spinal cord. All the animals sustained moderate compression through an aneurysm clip (30 g compressive force for 60 s), as described by Marques and coworkers [36]. After 24 h, SCI and SCI + PMMA groups were re-operated with the procedure above mentioned, exposing the damaged thoracic spinal cord. Only for SCI + PMMA group, a PMMA loaded AC gel-solution (5 μL) was placed with a micropipette on the damaged spinal cord, as presented in previous studies [37]. After spinal cord compression and gel positioning, dorsal muscles were juxtaposed using absorbable sutures and the skin sutured and disinfected. After the surgery, the animals were kept on a warm pad for 30 min and then placed in separated cages for recovery.

2.15. Transcardial perfusion

Mice were deeply anesthetized with Ketamine hydrochloride (Imalgene, 100 mg/kg, Alcyon Italia S.p.A.) and medetomidine hydrochloride (Domitor,1 mg/kg, Alcyon Italia S.p.A.) intraperitoneally injected and then transcardially perfused with 40 mL of sodium phosphate buffer (PBS) 0.1 mol/l pH 7.4, followed by 50 mL of 4% paraformaldehyde solution in PBS. Spinal cords were subsequently removed, post-fixed overnight in the same fixative, transferred to 30% sucrose in PBS at 4 °C for cryoprotection and stored at 4 °C until use.

2.16. Preparation of spinal cord sections

Spinal cord areas around the site of injection (±5 mm from the epicenter) were embedded in Tissue-Tek® O.C.T™ Compound (Sakura) and frozen by immersion in n-pentane at −45 °C for 3 min and then stored at −80 °C until use. Frozen tissues were sectioned in 30 μm coronal sections on a cryostat at −20 °C. Serial sections were collected in PBS with sodium azide (0.02%) and stored at 4 °C until use.

2.17. Immunofluorescence

Immunofluorescence was performed on 30 μm coronal spinal cord sections. Astrocyte staining was evaluated using a monoclonal antibody directed to GFAP (Glial Fibrillary Acidic Protein; mouse monoclonal anti-GFAP, 1:2500 dilution, Millipore, Italy) dissolved in PBS, 1% normal goat serum and 0.3% Triton and incubated overnight at 4 °C under constant shaking. Sections were then processed with anti-mouse secondary antibody conjugated to Alexa 647 (1:500 dilution, Invitrogen, Italy). Subsequently, a second staining using a rat monoclonal antibody anti-CD11b (specific for the complement C3 receptor of macrophages/monocytes/microglia, 1 μg/ml, homemade) was performed to detect microglia/macrophages cells. Sections were then incubated with a secondary anti-rat antibody conjugated to Alexa 488 (1:500 dilution, Invitrogen, Italy). To label neuronal cells, spinal cord sections were stained with NeuroTrace Fluorescent Nissl Stain (fluorescence excitation/emission maxima 640–660 nm, Invitrogen, Italy) dissolved in PBS for 10 min. Finally, spinal cord sections were mounted on slides and coverslipped with a 50% glycerol solution in PBS to proceed with the acquisition by confocal microscope.

2.18. Microscopy and fluorescence quantification

Colocalization studies were carried out by confocal microscope (40× objective magnification, BX81 microscope, FV1000 confocal; Olympus, Japan). Fluorescent NP signal was acquired (40× objective magnification, BX81 microscope and Fluoview II camera; Olympus, Japan) and bleed-through artifacts were avoided by using sequential acquisition with laser and filter settings here reported (Alexa 488, Laser 488, filter range 500–540; RhB, Laser 546, filter range 570–625; To-Pro3, Laser 646, filter range 650–750). To discriminate furthermore between intrinsic cell autofluorescence and specific signal for both RhB and To-Pro3 a linear spectral unmixing analysis was carried out (spectral unmixing module FV1000 confocal, Olympus, Japan).

Quantification was performed by Fiji (http://fiji.sc/Downloads) surrounding single cells (about 200) with the "free hand" selection and the integrated density of the signal was taken into consideration.

2.19. RhB and To-Pro3 quantification

Quantitative evaluation was performed using free software Fiji (http://fiji.sc/Downloads) and point picker tool (http://fiji.sc/Downloads). Single cells (about 200) were evaluated *in vivo* detecting RhB and To-Pro3 positive cells in a space corresponding to 600 μm of diameter around the injury site. A blind evaluation was performed by two different operators.

2.20. Statistical analysis

Data were processed using Prism 6 software (GraphPad, USA). Normality is evaluated by D'Agostino–Pearson normality test. We used non parametric test because data are not distributed normally. Mann–Whitney rank sum test was performed to test the significance among groups for both *in vitro* NP uptake assessment and MTS assay. Kruskal–Wallis and *post hoc* analysis (Dunn's test) were performed to test the significance among groups for *in vitro* NP uptake assessment after CPZ treatment and *in vitro* ELISA assay. $p < 0.05$ was considered as statistically significant for all the analysis.

3. Results

3.1. NP characterization

NPs were synthesized by emulsion free radical polymerization, which allows to control final PMMA-NPs features, in terms of size and surface charge [38]. The PMMA-NP characteristics, as measured by DLS, are listed in Table 1.

The produced NPs possess similar size and are monodispersed, as observable from polydispersity index data in Fig. 1A and TEM analysis in Fig. 1B. Different surface charges and PEGylations have been evaluated in this study and their characteristics are presented in Table 1. Furthermore, the NP stability in biological fluids was monitored for 72 h in cell culture medium. DLS analysis (see Table 1) did not reveal any alteration in terms of size and polydispersity for the whole duration of the experiment meaning that no aggregation took place and, consequently, that NPs are stable in the selected medium.

3.2. In vitro PMMA-NP selective uptake

Microglia, astrocytes and neurons obtained from the spinal cord of mouse embryos were used to study the uptake of PMMA-NPs. LPS-stimulation was used to activate microglia *in vitro*. LPS is a potent immuno-activator of monocytes and macrophages and it is widely used to activate microglial cells *in vitro*. LPS-stimulated microglial cells showed a hypertrophic shape (amoeboid/phagocytic shape) in comparison to unstimulated microglial cells (Fig. 2). Differently, no detectable morphological alterations were found for astrocytes and neuronal cells after the LPS stimulation (Fig. 2). After exposure of neuron/glia co-cultures to PMMA-NPs, a few internalized NPs were found selectively in unstimulated CD11b positive microglial cells (Fig. 2). However, when we analyzed the LPS-stimulated co-cultures, a remarkable increase in PMMA-NP uptake was detected, as shown by a higher diffuse RhB signal in the cytosol of activated microglia (Fig. 2c,d).

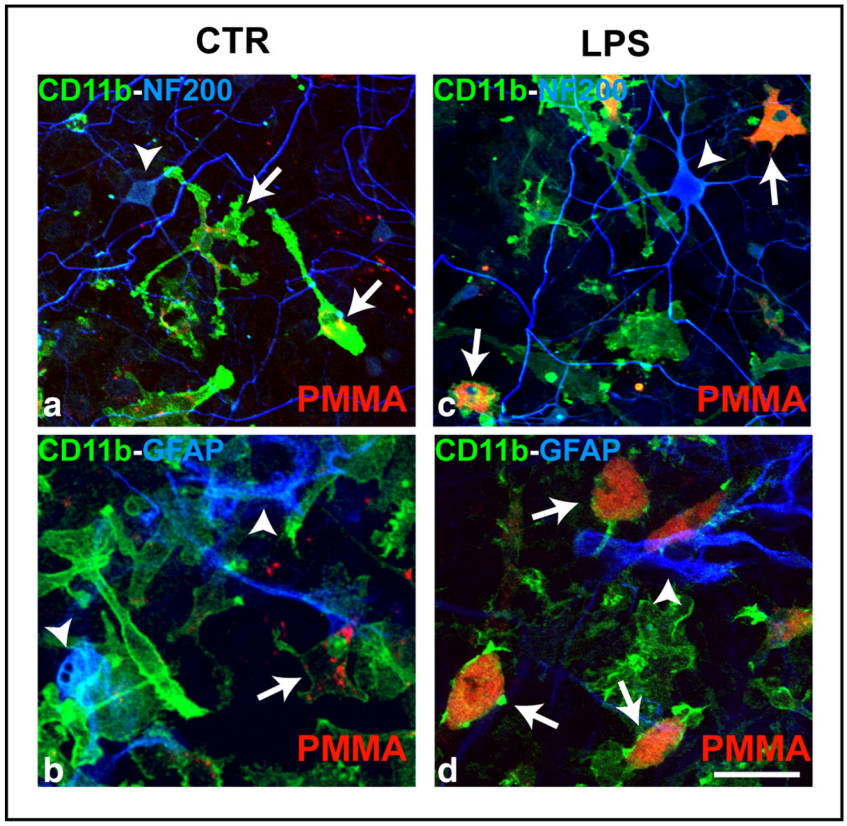

Fig. 2. PMMA-NP uptake and distribution *in vitro*. In LPS-stimulated cells (c–d) microglia show a hypertrophic phenotype compared to control condition (a–b). Accumulation of fluorescent PMMA-NPs is markedly increased in LPS-stimulated microglial cells (c–d, arrows) compared to control condition (a–b, arrows). No internalization is observed in either astrocytes (a,c arrowheads) or neurons (b,d arrowheads). Scale bar = 15 μm.

3.3. In vitro time-lapse analysis of PMMA-NP uptake with charge and PEGylation variants

In time lapse analysis, PMMA-NPs exhibited a very rapid internalization in microglial cells (already detectable after 30 min) with a plateau after 3 h of treatment (Fig. 3A,B). After PMMA-NP internalization, a cytosolic localization of the RhB signal was found in activated microglia, progressively evolving in a cytosol-perinuclear intense distribution, as revealed at the end of the acquisition (Fig. 3A). To investigate the contribution of different chemical and physical variants on the uptake kinetics of polymeric PMMA-NPs by LPS-stimulated microglia, time-lapse analysis was performed. PMMA-NPs were compared to positively charged-PMMA (PMMA_pos) by quantitative analysis after 3 h of incubation. A significantly increased uptake of PMMA_pos was again revealed in LPS-stimulated compared to unstimulated microglia (Fig. 3C). However, it is worth to emphasize that the difference in PMMA-NP internalization between LPS-stimulated and unstimulated microglia (CTR) was higher for PMMA_pos (2.3 fold) than for PMMA-NPs (2.0 fold). In line with this result, the internalization in LPS-stimulated microglia of PMMA_pos NPs was significantly higher (4.83 ± 5.3 mean integrated density ± SD) than that of PMMA-NPs (3.46 ± 4.53 mean integrated density ± SD). This result demonstrates that the surface charge has a role in the uptake kinetics of such NPs.

To investigate whether the presence of polyethylene glycol (PEG) chains were able to affect the internalization kinetics of PMMA-NPs, we quantitatively evaluated the cytosolic levels of PEGylated PMMA (PMMA_PEG), in comparison to non-PEGylated NPs, after 3 and 48 h of exposure. After 3 h of incubation, the quantification of the RhB signal in the cytosol of LPS-stimulated microglia showed that PMMA_PEG internalization was significantly lower (by about 1.5-fold) (2.25 ± 3.10 mean integrated intensity ± SD) compared to NPs without PEGylation (3.46 ± 4.53 mean integrated intensity ± SD). However, an increased RhB signal was found after 48 h of incubation with PMMA_PEG (4.36 ± 4.96 mean integrated intensity ± SD) (Fig. 3D), demonstrating that PEG chains linked to PMMA-NPs slow down the NP uptake by microglia, but do not block their internalization.

3.4. Uptake mechanism and cell viability

To investigate the mechanism underlying the PMMA-NP internalization, we tested a specific clathrin-mediated endocytosis inhibitor, chlorpromazine (CPZ). LPS-stimulated co-cultures were pre-treated for 2 h, before the exposure to PMMA-NPs, with different concentrations of CPZ (30, 40 and 50 μM). The NP uptake evaluation was performed only in healthy glial cells detected as negative staining for propidium iodide (cell death marker). A significant dose-dependent inhibition of PMMA-NP uptake in LPS-stimulated microglia was induced by 30 (2.89 ± 2.55 mean integrated intensity ± SD) and 40 μM (1.30 ± 1.52 mean integrated intensity ± SD) of CPZ compared to LPS-stimulated cells not treated with CPZ (5.61 ± 5.18 mean integrated intensity ± SD) (Fig. 4A,B). Fifty μM CPZ showed a cytotoxic effect (data not shown).

To determine whether the internalized PMMA-NPs were able to modify the microglial viability we measured the cell vitality in purified microglia cultures by MTS assay. PMMA-NP internalization did not affect LPS-stimulated microglial cell viability up to 6 days compared to LPS-stimulated microglia not exposed to NPs (Fig. 4C). To understand whether internalized PMMA-NPs affected the cytokine release from LPS-stimulated co-cultures, we measured the levels of IL-1β, TNFα and IL-6 in the medium of microglial cells. An ELISA assay for these cytokines was performed after 24 h of exposure to NPs after the removal of the LPS stimulus. No detectable amount of IL-1β and TNFα cytokines

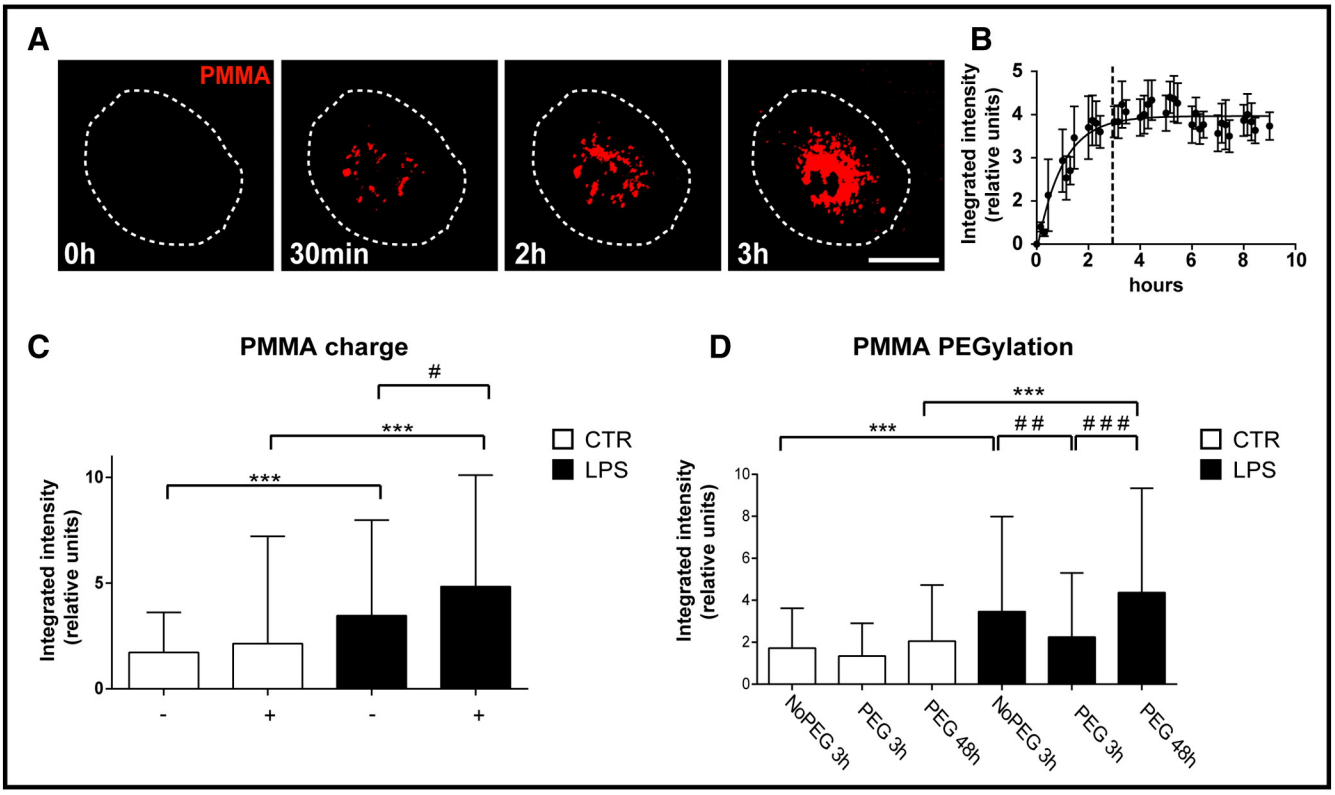

Fig. 3. Time-lapse analysis of PMMA-NPs by LPS-stimulated microglia. (A,B) PMMA-NPs (red signal) progressively accumulate in the cytosol reaching a plateau after 3 h of incubation. (C) Uptake quantification of PMMA-NPs having charge variants (positive or negative), in LPS-stimulated (LPS) *vs* unstimulated microglia (CTR). PMMA-NPs show a significantly increased internalization in LPS-stimulated cells compared to CTR and this is more pronounced in PMMA_pos (about 2.3-fold compared to a 2.0 fold increase in PMMA-NPs) after 3 h of treatment. (D) Uptake quantification of PEGylated (PEG) or non-PEGylated PMMA-NPs in LPS-stimulated (LPS) *vs* unstimulated (CTR) microglia. PEGylation slows down the PMMA-NPs internalization, but does not block it. Scale bar = 10 μm. Data are presented as mean ± SD. Statistical significance: (***)$p < 0.001$, (#)$p < 0.05$, (##)$p < 0.01$ and (###)$p < 0.001$.

was found in LPS stimulated cells at this time of detection. Contrarily, IL-6 showed significantly increased levels in the medium of LPS stimulated co-cultures (288.9 ± 73.12 pg/ml mean ± SD) compared to unstimulated cells (34.2 ± 7.8 pg/ml mean ± SD) (Fig. 4D). However, there were no significant differences in IL-6 release between microglial cells exposed (305.4 ± 102.1 pg/ml mean ± SD) and not exposed (288.9 ± 73.12 pg/ml mean ± SD) to NPs (Fig. 4D).

3.5. In vitro drug delivery

To further understand whether polymeric NPs were able to deliver encapsulated compounds into the cytosol of activated microglia, PMMA-NPs were loaded with To-Pro3 (PMMA-To-Pro3), a far-red fluorophore, here used as a drug mimetic compound. To-Pro3 is a cell membrane impermeable compound that is not able to pass the intact membrane of viable cells. The colocalization of single fluorescent RhB-positive PMMA-NPs (red signal) loaded with To-Pro3 (blue signal) showed that the mimetic drug was efficiently encapsulated (Fig. 5A). The loading percentage of To-Pro3 within PMMA NPs was 82.5 ± 2.5% as detected by spectroscopy. The release of To-Pro3 from NPs was investigated after incubating the PMMA NPs at 37 °C. To-Pro3 release, as showed from Fig. 5B,a, followed a biphasic pattern characterized by an initial burst release followed by a slower sustained release phase that was observed during 14 days. The percentage of To-Pro3 released in the first 2 h (around 25%) can be attributed to the unloaded To-Pro3 and to the high initial concentration gradient present. Thereon, To-Pro3 was slowly released through a pure Fickian diffusion phenomenon as evident from Fig. 5B.b, where a linear relationship between percentage released and square root time was observed. These results confirm that the release from PMMA NPs is still mediated by Fickian diffusion. To evaluate the To-Pro3 delivery by PMMA NPs *in vitro* the NPs were incubated for 24 h with LPS-stimulated microglial cells. At this time of analysis, LPS-stimulated microglia showed clusterized PMMA-NPs in the cytosol with a colocalized RhB and To-Pro3 signals (Fig. 5C). After 5 days of incubation, a markedly diffused signal of To-Pro3 was revealed in the cytosol of the LPS-stimulated microglial cells and it was only partially colocalized with RhB (Fig. 5C). This is more evident with pseudocolor image, where To-Pro3 signal was more widespread diffused within the cytosol, compared to RhB-positive PMMA-NPs (Fig. 5C). To confirm that the internalization and delivery of To-Pro3 carried by PMMA-NPs occurred after crossing intact membranes of viable cells, a subsequent staining with propidium iodide (PI) was performed on microglia containing PMMA-To-Pro3 (data not shown). PI is a marker used to test the integrity of cellular membrane (positive staining of PI in the nucleus of the cells suggests a compromised integrity of the cellular membrane). PI test showed a lack of staining in cells containing both RhB and To-Pro3 positive NPs, confirming an internalization of To-Pro3 which can only be carried by NPs in viable microglia.

3.6. In vivo NP uptake and drug delivery

In order to test and characterize the distribution and uptake of PMMA-NPs *in vivo*, an injection of a solution of hydrogel containing NPs was performed into the parenchyma of mouse spinal cord (see Materials and methods). After the injection, the hydrogel revealed a spherical enclosure in the spinal cord in a very short time (minutes) due to its *in situ* gelation that physically displaced the parenchyma. To evaluate the inflammatory response of the tissue to the injury induced by the injected hydrogel, a double staining with markers for microglia and astrocytes, respectively CD11b and GFAP, was carried out. An inflammatory reaction was detected around the hydrogel at 3 days post-injection (DPI), identified as a glial scar formation composed of

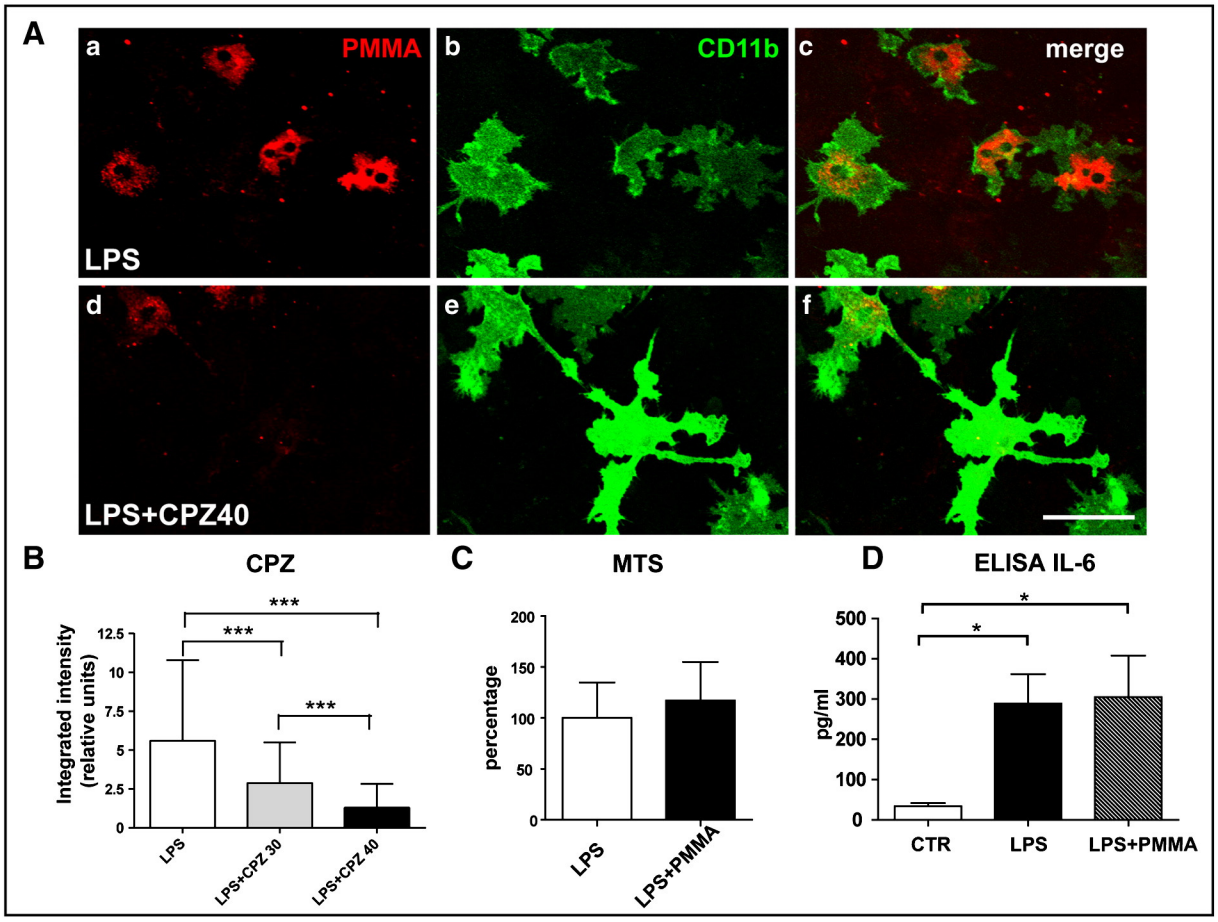

Fig. 4. (A) NPs are internalized by clathrin-mediated endocytosis in LPS-stimulated microglia. Pre-treatment with chlorpromazine (CPZ) (d–f) inhibits NPs uptake by activated microglia *in vitro*. (B) Quantitative analysis shows that uptake inhibition of PMMA-NPs by CPZ occurs in a dose-dependent manner. (C) MTS assay reveals that viability of LPS-stimulated microglial cells after 6 days of treatment with NPs is not affected. Data are presented as percentage ± SD of viable cells normalized to LPS treatment condition (not exposed to NPs). (D) ELISA assay performed on the supernatants of LPS stimulated cells shows that after NPs treatment, the release of pro-inflammatory cytokine IL-6 induced by LPS stimulation is not significantly altered. Data are presented as mean ± SD. Statistical significance: (*)$p < 0.05$ and (***) $p < 0.001$. Scale bar = 10 μm.

phagocytic/ameboid microglia (Fig. 6A,B). A distribution of PMMA-NPs was revealed around the injected hydrogel showing a selective uptake in the surrounding activated-phagocytic microglia/macrophages (Fig. 6A,B). The selective uptake by the microglia/macrophages was confirmed by the lack of colocalization between PMMA-NPs and GFAP/Neurotrace (Fig. 6B). Furthermore, to demonstrate the capacity of PMMA-NPs to deliver encapsulated compounds, the mimetic drug To-Pro3 was loaded in PMMA-NPs, which in turn were injected together with the hydrogel in mouse spinal cord. A diffused To-Pro3 signal was detected in activated microglia/macrophages that have taken up PMMA-NPs at 3DPI (Fig. 6D). This was revealed for different activated forms of microglial cells, identified by their own morphological features: ameboid-like, having a short ramified shape, or phagocytic-like, showing a round shape phenotype (Fig. 6C). The latter showed a more diffuse To-Pro3 signal in comparison to ameboid-like microglial cells, likely reflecting an increased uptake of PMMA-NPs (Fig. 6C,D). To determine the percentage of microglia/macrophages that have taken up NPs, a quantitative evaluation around the injury site was performed detecting the number of positive macrophage/microglial cells for both RhB and To-Pro3 (61.2 ± 6.5 mean ± standard deviation of evaluated cells) (Fig. 6E,a). Furthermore, a quantitative evaluation of the colocalization of To-Pro3 and RhB signal was carried out showing a partial colocalized signal between them (about 50%) at this time of analysis, as demonstrated by the correlation coefficient units for two different evaluated parameters, Pearson and Manders. This result confirms that at least the 50% of the mimetic drug was released in microglia/macrophages already at 3DPI (Fig. 6E,b).

3.7. Behavioral evaluation

The CTR group did not show any functional alteration evaluated by Basso Mouse Scale (BMS). SCI animals showed flaccid paralysis 24 h after injury, with a subsequent modest improvement during the following weeks, reaching a score of 3.2 ± 2.0 (mean ± standard deviation) at 28 DPI. Analyzing injured animals treated with PMMA (SCI + PMMA) a comparable locomotor improvement was found, compared to SCI group, reaching a score of 3.5 ± 1.9 (mean ± standard deviation) at 28 DPI (Fig. 7). The maximum score (BMS = 9) was obtained only by CTR group (Fig. 7). As expected, significant differences were found comparing CTR group to either SCI or SCI + PMMA groups, at all the time points evaluated after clip compression ($p < 0.001$), but none between SCI and SCI + PMMA groups (Fig. 7).

4. Discussion

In this study we characterized a new pharmacological delivery tool (PMMA-NPs) able to enter specifically in activated microglia/macrophages and to release mimetic-drug compounds (To-Pro3), both *in vitro* and *in vivo*. Specifically, we demonstrated that: I) PMMA-NPs are internalized selectively by microglial cells in a very short time (some hours); II) microglia in activated form are able to internalize markedly PMMA-NPs, whereas microglia displaying a resting phenotype are not; III) PMMA-NPs offer the advantage to have tunable surface charge and PEGylation allowing to modify and adjust the amount of NPs internalized by microglia/macrophages in accordance with the need of

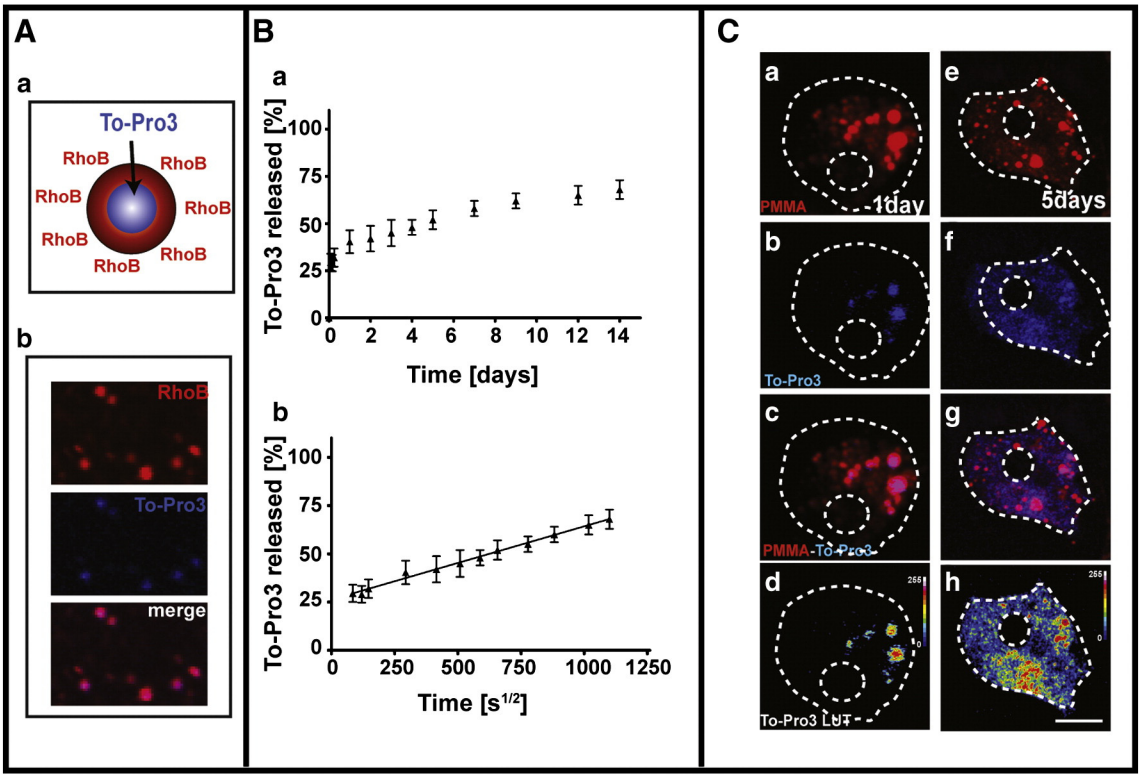

Fig. 5. To-Pro3 delivery from NPs after internalization in LPS-stimulated microglia. (A) Colocalization of isolated fluorescent RhB-positive PMMA-NPs (red signal) loaded with To-Pro3 (blue signal) shows that the mimetic drug is encapsulated in NPs. (B) *In vitro* release profile of To-Pro3 delivered from NPs (a). The slope of To-Pro3 release from NPs against the square root time is representative of Fickian diffusion coefficient of NPs in gels ($p < 0.0001$). Diffusion controlled release is sustained for 14 days. Values are calculated as percentage respect to the total mass loaded (mean value ± standard deviation are plotted) (b). (C) LPS-stimulated microglial cells show a colocalized signal between To-Pro3 and RhB positive PMMA-NPs in the cytosol after 24 h of exposure (a–d). A markedly diffused signal of To-Pro3 is evident in the cytosol of the LPS-stimulated microglial cells after 5 days from the NP internalization (e–h). Representative To-Pro3 intensity using pseudocolor (d,h). Scale bar = 5 μm.

the drug to be released; IV) PMMA-NP internalization in activated microglial cells is based on clathrin-dependent endocytosis mechanisms; VI) PMMA-NPs do not induce toxicity after the uptake in microglia/macrophages; VII) PMMA-NPs tested are able to deliver efficiently mimetic drug (To-Pro3) in the cytosol of activated microglial cells *in vitro* and *in vivo*. To-Pro3 is a near-infrared fluorescent molecule that could be considered a model, in terms of steric hindrance and lipophilicity, for drugs with similar chemical properties, such as pioglitazone [39–42], minocycline [43–45] and rolipram [46], which have shown the capacity to modulate activated microglia/macrophages in different model systems. To-Pro3 is not able to cross the cell membrane of vital cells by itself. Hence, To-Pro3 is an optimal candidate for studying the carrier properties of PMMA-NPs.

Microglia are able to rapidly respond to pathological insults adopting an activated morphology (amoeboid or phagocytic shape). Recently, much evidence suggested a dual role (M1—harmful or M2—beneficial) of activated microglia/macrophages during the progression of the secondary injury. An imbalance between these two subsets (M1/M2) likely determines the beneficial or detrimental development of the inflammatory response in the secondary injury, leading to resolution or exacerbation of the pro-inflammatory stimulus. Detrimental effects have been associated to the M1 phenotype such as the production of pro-inflammatory mediators including cytokines (IL1β, IL-6 and TNFα), oxygen radicals and inducible nitric oxide synthase, that contribute to the cascade of inflammatory events during the secondary injury [12,13]. Recent findings have highlighted the involvement of harmful activated microglia also in the persisting pain state of SCI. Indeed, spinal cord microglia are strongly activated in different pain mouse models [47] showing morphological changing toward an ameboid-like phenotype and elevated phosphorylation of p38 mitogen-activated protein kinase. This in turn may increase the synthesis of proinflammatory cytokines (IL-1β, IL-6, TNF-α) [48] and factors (brain derived neurotrophic factor) [49] which are able to modulate the excitability of dorsal horn neurons contributing to chronic pain symptoms. On the other side, microglia/macrophages activation, characterized by a pleiotropic effect, showed also a beneficial role during the progression of the secondary injury (M2 phenotype) [12]. This includes protective effects in terms of repair and resolution of inflammation and it is identified by an upregulation of arginase 1, YM1 and CD206 [50]. Unfortunately, M2 represents only a transient expression in a subacute phase in the progression of the secondary injury, limiting the beneficial effects to a temporally restricted phase (some days from the injury) [12]. On the contrary, M1 phenotype showed an early and persistent activation in both subacute and chronic phases of SCI [12]. This suggests that persistent microglia/macrophages associated inflammation is a relevant mechanism in the progression of the secondary injury representing a crucial therapeutic target for SCI treatment.

Different strategies aimed to selectively modulate microglia have already been proposed in preclinical paradigms, such as specific viral carriers able to transfer genetic sequences and modulate their own expression [51] or various anti-inflammatory treatments [11,43]. However, they showed many limitations. Some safety concerns are associated with gene therapy approaches. Moreover the short half-life of genes delivered in diving cells through non-integrative vectors and the possibility that the viral vector is inactivated due to recognition by the immune system restrict the range of possible applications of gene therapy [52]. On the other hand, anti-inflammatory drugs are not selective for a specific cell type and may give rise to potential side effects associated with systemic administration. Recently, a new approach using a NP-based tool has been proposed as a selective carrier to deliver

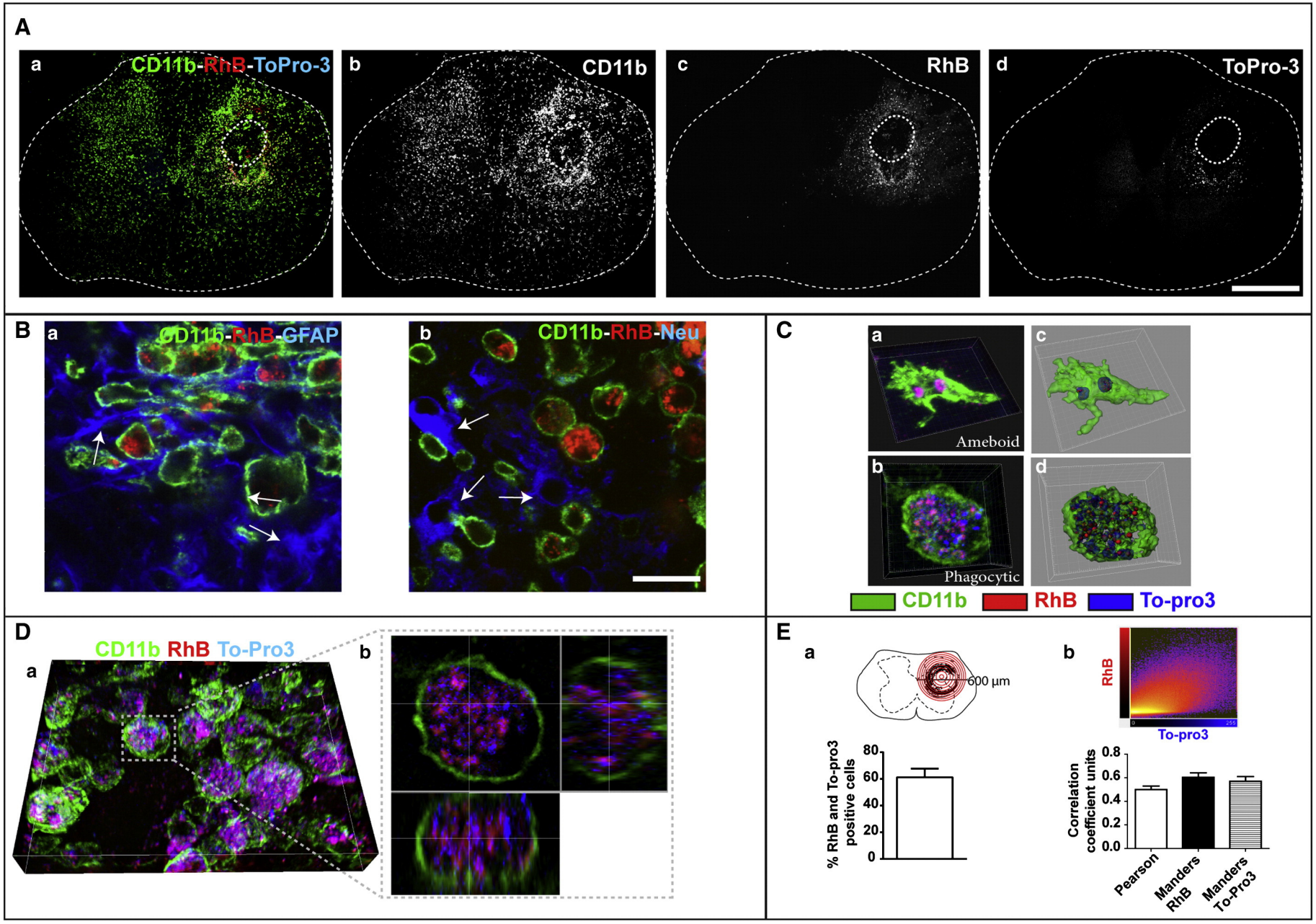
A
a
CD11b-RhB-ToPro-3
b
CD11b
c
RhB
d
ToPro-3
B
a
CD11b-RhB-GFAP
b
CD11b-RhB-Neu
C
a
c
Ameboid
b
d
Phagocytic
CD11b
RhB
To-pro3
D
CD11b RhB To-Pro3
a
b
E
a
600 µm
% RhB and To-pro3 positive cells
80
60
40
20
0
b
RhB
To-pro3
Correlation coefficient units
0.8
0.6
0.4
0.2
0.0
Pearson
Manders RhB
Manders To-Pro3

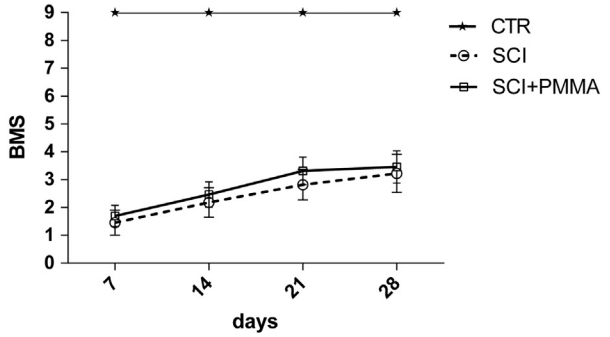

Fig. 7. Basso Mouse Scale (BMS) test to evaluate the potential toxicity of PMMA-based NPs on behavioral outcome. Healthy animals (CTR) have been compared to either traumatized mice (SCI) or injured mice treated with PMMA (SCI + PMMA). No significant differences were detected in BMS between SCI group and SCI + PMMA mice (n = 13 mice for each group evaluated). Data are presented as mean ± standard deviation.

compounds directly in microglial cells, namely Qdot nanocrystal [53]. However, a great limitation associated with the capability of these NPs to link chemically compounds restricts this approach to a scantly number of drugs. On the basis of that, new strategies are needed to counteract the propagation of the secondary inflammatory response and the development of post-traumatic chronic pain due to the activated microglia/macrophages. In this paper we validate a new pharmacological approach, based on polymeric NPs, that is able to selectively target activated microglial cells *in vitro* and *in vivo*. This may represent a potential tool able to modulate selectively microglia/macrophages activation in SCI. The selective and specific treatment here proposed shows, compared to the conventional anti-inflammatory therapy, some potential advantages: I) an improved efficacy of treatment by increasing the concentration of the drug in specific target cells in the site of injury; II) reduced potential side effects due to the possibility to avoid unwanted distribution of the drug to not-target tissues; III) time-selective treatment of microglial cells offers the potential to modulate the activation of the microglial cells at different stages of the secondary injury and possibly to deepen the understanding of the detrimental or beneficial role of the microglia during the progression of the disease.

5. Conclusions

In this work we demonstrated the possibility to target drugs loaded in NPs in a specific cell population (activated microglia/macrophages), involved in the post-traumatic degeneration of the spinal cord. PMMA-NPs were internalized selectively by LPS-activated microglia, without any toxic effect. We considered different tunable parameters (surface charge and PEGylation) that allow to control cell uptake. *In vitro* and *in vivo* studies showed selective drug release within cell cytosol of activated microglia/macrophages confirming the efficacy of this tool. In conclusion, the approach proposed in this work is potentially able to treat inflammatory microglia/macrophages in SCI and may provide benefit in different human neurologic diseases opening new perspectives to the inflammatory treatment in the central nervous system.

Acknowledgments

This study was supported by the Fondazione Cariplo, grant no. 2010/0639.

References

[1] R. Ben Borgens, P. Liu-Snyder, Understanding secondary injury, Q. Rev. Biol. 87 (2012) 89–127.
[2] L.S. Illis, Central nervous system regeneration does not occur, Spinal Cord 50 (2012) 259–263.
[3] S. Thuret, L.D. Moon, F.H. Gage, Therapeutic interventions after spinal cord injury, Nat. Rev. Neurosci. 7 (2006) 628–643.
[4] G.W.J. Hawryluk, J. Rowland, B.K. Kwon, M.G. Fehlings, Protection and repair of the injured spinal cord: a review of completed, ongoing, and planned clinical trials for acute spinal cord injury, Neurosurg. Focus. 25 (2008).
[5] G. Onose, A. Anghelescu, D.F. Muresanu, L. Padure, M.A. Haras, C.O. Chendreanu, L.V. Onose, A. Mirea, A.V. Ciurea, W.S. El Masri, K.R.H. von Wild, A review of published reports on neuroprotection in spinal cord injury, Spinal Cord 47 (2009) 716–726.
[6] B.K. Kwon, L.H. Sekhon, M.G. Fehlings, Emerging repair, regeneration, and translational research advances for spinal cord injury, Spine (Phila Pa 1976) 35 (2010) S263–S270.
[7] B.K. Kwon, E. Okon, J. Hillyer, C. Mann, D. Baptiste, L.C. Weaver, M.G. Fehlings, W. Tetzlaff, A systematic review of non-invasive pharmacologic neuroprotective treatments for acute spinal cord injury, J. Neurotrauma 28 (2011) 1545–1588.
[8] S. David, J.G. Zarruk, N. Ghasemlou, Inflammatory pathways in spinal cord injury, Int. Rev. Neurobiol. 106 (2012) 127–152.
[9] K.D. Beck, H.X. Nguyen, M.D. Galvan, D.L. Salazar, T.M. Woodruff, A.J. Anderson, Quantitative analysis of cellular inflammation after traumatic spinal cord injury: evidence for a multiphasic inflammatory response in the acute to chronic environment, Brain 133 (2010) 433–447.
[10] A. Sierra, O. Abiega, A. Shahraz, H. Neumann, Janus-faced microglia: beneficial and detrimental consequences of microglial phagocytosis, Front. Cell. Neurosci. 7 (2013) 6.
[11] D.J. Loane, K.R. Byrnes, Role of microglia in neurotrauma, Neurotherapeutics 7 (2010) 366–377.
[12] K.A. Kigerl, J.C. Gensel, D.P. Ankeny, J.K. Alexander, D.J. Donnelly, P.G. Popovich, Identification of two distinct macrophage subsets with divergent effects causing either neurotoxicity or regeneration in the injured mouse spinal cord, J. Neurosci. 29 (2009) 13435–13444.
[13] R. Shechter, O. Miller, G. Yovel, N. Rosenzweig, A. London, J. Ruckh, K.W. Kim, E. Klein, V. Kalchenko, P. Bendel, S.A. Lira, S. Jung, M. Schwartz, Recruitment of beneficial M2 macrophages to injured spinal cord is orchestrated by remote brain choroid plexus, Inmmunity 38 (2013) 555–569.
[14] S.R. Cerqueira, J.M. Oliveira, N.A. Silva, H. Leite-Almeida, S. Ribeiro-Samy, A. Almeida, J.F. Mano, N. Sousa, A.J. Salgado, R.L. Reis, Microglia response and in vivo therapeutic potential of methylprednisolone-loaded dendrimer nanoparticles in spinal cord injury, Small 9 (2013) 738–749.
[15] A. Sato, H. Ohtaki, T. Tsumuraya, D. Song, K. Ohara, M. Asano, Y. Iwakura, T. Atsumi, S. Shioda, Interleukin-1 participates in the classical and alternative activation of microglia/macrophages after spinal cord injury, J. Neuroinflammation 9 (2012) 65.
[16] L. Florez, C. Herrmann, J.M. Cramer, C.P. Hauser, K. Koynov, K. Landfester, D. Crespy, V. Mailander, How shape influences uptake: interactions of anisotropic polymer nanoparticles and human mesenchymal stem cells, Small 8 (2012) 2222–2230.
[17] J. Nicolas, S. Mura, D. Brambilla, N. Mackiewicz, P. Couvreur, Design, functionalization strategies and biomedical applications of targeted biodegradable/biocompatible polymer-based nanocarriers for drug delivery, Chem. Soc. Rev. 42 (2013) 1147–1235.
[18] F. Rossi, G. Perale, S. Papa, G. Forloni, P. Veglianese, Current options for drug delivery to the spinal cord, Expert Opin. Drug Deliv. 10 (2013) 385–396.
[19] J.C. Stanwick, M.D. Baumann, M.S. Shoichet, Enhanced neurotrophin-3 bioactivity and release from a nanoparticle-loaded composite hydrogel, J. Control. Release 160 (2012) 666–675.
[20] Y.C. Kuo, H.F. Ko, Targeting delivery of saquinavir to the brain using 83-14 monoclonal antibody-grafted solid lipid nanoparticles, Biomaterials 34 (2013) 4818–4830.
[21] I. Canton, G. Battaglia, Endocytosis at the nanoscale, Chem. Soc. Rev. 41 (2012) 2718–2739.
[22] D. Di Mascolo, C. Lyon, S. Aryal, M.R. Ramirez, J. Wang, P. Candeloro, M. Guindani, W.A. Hsueh, P. Decuzzi, Rosiglitazone-loaded nanospheres for modulating macrophage-specific inflammation in obesity, J. Control. Release 170 (2013) 460–468.
[23] G. Sharma, D.T. Valenta, Y. Altman, S. Harvey, H. Xie, S. Mitragotri, J.W. Smith, Polymer particle shape independently influences binding and internalization by macrophages, J. Control. Release 147 (2010) 408–412.
[24] C. He, L. Yin, C. Tang, C. Yin, Multifunctional polymeric nanoparticles for oral delivery of TNF-alpha siRNA to macrophages, Biomaterials 34 (2013) 2843–2854.
[25] N.K. Jain, V. Mishra, N.K. Mehra, Targeted drug delivery to macrophages, Expert Opin. Drug Deliv. 10 (2013) 353–367.
[26] C. Colombo, M. Lupi, P. Ubezio, D. Moscatelli, Cytotoxicity of PMMA-based nanoparticles synthesized adopting SDS and Tween80, Macromol. Symp. 324 (2013) 134–139.
[27] L. Cova, P. Bigini, V. Diana, L. Sitia, R. Ferrari, R.M. Pesce, R. Khalaf, P. Bossolasco, P. Ubezio, M. Lupi, M. Tortarolo, L. Colombo, D. Giardino, V. Silani, M. Morbidelli, M.

Fig. 6. PMMA-NPs are able to deliver To-Pro3 in activated microglia already at 3DPI *in vivo*. (A) Low magnification of coronal section of mouse spinal cord injected with hydrogel shows an activated microglia/macrophages (CD11b staining) around the site of injection and a microglia/macrophages uptake of PMMA-To-Pro3 (a–d). Scale bar = 150 μm. (B) High magnification of astrocytes, microglia and neuronal cells staining around the injury site. PMMA-NP internalization is evident only in CD11b positive microglia/macrophages, but not in astrocytes (a) and neuronal cells (b). Scale bar = 15 μm. (C) 3D Isosurface reconstruction of To-Pro3 delivery from PMMA-NPs in both ameboid and phagocytic microglia/macrophages. (D) 3D reconstruction (a) and orthogonal projection (b) of To-Pro3 delivery from PMMA-NPs in activated microglia/macrophages. (E) Percentage of both RhB and ToPro-3 positive cells evaluated in 600 μm of diameter of injured site (a). Pearson and Manders evaluation of the To-Pro3 and RhB colocalization in microglia/macrophages (b).

Salmona, D. Moscatelli, Biocompatible fluorescent nanoparticles for in vivo stem cell tracking, Nanotechnology 24 (2013) 245603.
[28] J. Jung, I.-H. Lee, E. Lee, J. Park, S. Jon, pH-sensitive polymer nanospheres for use as a potential drug delivery vehicle, Biomacromolecules 8 (2007) 3401–3407.
[29] A. Bettencourt, A.J. Almeida, Poly(methyl methacrylate) particulate carriers in drug delivery, J. Microencapsul. 29 (2012) 353–367.
[30] M. Dossi, R. Ferrari, L. Dragoni, C. Martignoni, P. Gaetani, M. D'Incalci, M. Morbidelli, D. Moscatelli, Synthesis of fluorescent PMMA-based nanoparticles, Macromol. Mater. Eng. 298 (2013) 771–778.
[31] R. Ferrari, C. Colombo, C. Casali, M. Lupi, P. Ubezio, F. Falcetta, M. D'Incalci, M. Morbidelli, D. Moscatelli, Synthesis of surfactant free PCL-PEG brushed nanoparticles with tunable degradation kinetics, Int. J. Pharm. 453 (2013) 551–559.
[32] M. De Paola, V. Diana, P. Bigini, T. Mennini, Morphological features and responses to AMPA receptor-mediated excitotoxicity of mouse motor neurons: comparison in purified, mixed anterior horn or motor neuron/glia cocultures, J. Neurosci. Methods 170 (2008) 85–95.
[33] M. De Paola, A. Mariani, P. Bigini, M. Peviani, G. Ferrara, M. Molteni, S. Gemma, P. Veglianese, V. Castellaneta, V. Boldrin, C. Rossetti, C. Chiabrando, G. Forloni, T. Mennini, R. Fanelli, Neuroprotective effects of toll-like receptor 4 antagonism in spinal cord cultures and in a mouse model of motor neuron degeneration, Mol. Med. 18 (2012) 971–981.
[34] G. Perale, F. Rossi, M. Santoro, M. Peviani, S. Papa, D. Llupi, P. Torriani, E. Micotti, S. Previdi, L. Cervo, E. Sundstrom, A.R. Boccaccini, M. Masi, G. Forloni, P. Veglianese, Multiple drug delivery hydrogel system for spinal cord injury repair strategies, J. Control. Release 159 (2012) 271–280.
[35] F. Rossi, M. Santoro, T. Casalini, P. Veglianese, M. Masi, G. Perale, Characterization and degradation behavior of agar-carbomer based hydrogels for drug delivery applications: solute effect, Int. J. Mol. Sci. 12 (2011) 3394–3408.
[36] S.A. Marques, V.F. Garcez, E.A. Del Bel, A.M. Martinez, A simple, inexpensive and easily reproducible model of spinal cord injury in mice: morphological and functional assessment, J. Neurosci. Methods 177 (2009) 183–193.
[37] F. Rossi, R. Ferrari, S. Papa, D. Moscatelli, T. Casalini, G. Forloni, G. Perale, P. Veglianese, Tunable hydrogel-nanoparticles release system for sustained combination therapies in the spinal cord, Colloids Surf. B: Biointerfaces 108 (2013) 169–177.
[38] R. Ferrari, Y.C. Yu, M. Morbidelli, R.A. Hutchinson, D. Moscatelli, Epsilon-caprolactone-based macromonomers suitable for biodegradable nanoparticles synthesis through free radical polymerization, Macromolecules 44 (2011) 9205–9212.
[39] A.R. Carta, A. Pisanu, Modulating microglia activity with PPAR-gamma agonists: a promising therapy for Parkinson's disease? Neurotox. Res. 23 (2013) 112–123.
[40] E. Gray, M. Ginty, K. Kemp, N. Scolding, A. Wilkins, The PPAR-gamma agonist pioglitazone protects cortical neurons from inflammatory mediators via improvement in peroxisomal function, J. Neuroinflammation 9 (2012) 63.
[41] H. Ji, H. Wang, F. Zhang, X. Li, L. Xiang, S. Aiguo, PPARgamma agonist pioglitazone inhibits microglia inflammation by blocking p38 mitogen-activated protein kinase signaling pathways, Inflamm. Res. 59 (2010) 921–929.
[42] S. Mandrekar-Colucci, J.C. Karlo, G.E. Landreth, Mechanisms underlying the rapid peroxisome proliferator-activated receptor-gamma-mediated amyloid clearance and reversal of cognitive deficits in a murine model of Alzheimer's disease, J. Neurosci. 32 (2012) 10117–10128.
[43] B.W. Festoff, S. Ameenuddin, P.M. Arnold, A. Wong, K.S. Santacruz, B.A. Citron, Minocycline neuroprotects, reduces microgliosis, and inhibits caspase protease expression early after spinal cord injury, J. Neurochem. 97 (2006) 1314–1326.
[44] B.C. Hains, S.G. Waxman, Activated microglia contribute to the maintenance of chronic pain after spinal cord injury, J. Neurosci. 26 (2006) 4308–4317.
[45] K. Kobayashi, S. Imagama, T. Ohgomori, K. Hirano, K. Uchimura, K. Sakamoto, A. Hirakawa, H. Takeuchi, A. Suzumura, N. Ishiguro, K. Kadomatsu, Minocycline selectively inhibits M1 polarization of microglia, Cell Death Dis. 4 (2013) e525.
[46] M. Ghosh, D. Garcia-Castillo, V. Aguirre, R. Golshani, C.M. Atkins, H.M. Bramlett, W.D. Dietrich, D.D. Pearse, Proinflammatory cytokine regulation of cyclic AMP-phosphodiesterase 4 signaling in microglia in vitro and following CNS injury, Glia 60 (2012) 1839–1859.
[47] Y.S. Gwak, J. Kang, G.C. Unabia, C.E. Hulsebosch, Spatial and temporal activation of spinal glial cells: role of gliopathy in central neuropathic pain following spinal cord injury in rats, Exp. Neurol. 234 (2012) 362–372.
[48] R. Vallejo, D.M. Tilley, L. Vogel, R. Benyamin, The role of glia and the immune system in the development and maintenance of neuropathic pain, Pain Pract. 10 (2010) 167–184.
[49] T. Trang, S. Beggs, M.W. Salter, ATP receptors gate microglia signaling in neuropathic pain, Exp. Neurol. 234 (2012) 354–361.
[50] S. David, A. Kroner, Repertoire of microglial and macrophage responses after spinal cord injury, Nat. Rev. Neurosci. 12 (2011) 388–399.
[51] J. Chen, Y. Zhou, S. Mueller-Steiner, L.F. Chen, H. Kwon, S. Yi, L. Mucke, L. Gan, SIRT1 protects against microglia-dependent amyloid-beta toxicity through inhibiting NF-kappaB signaling, J. Biol. Chem. 280 (2005) 40364–40374.
[52] N. Nayerossadat, T. Maedeh, P.A. Ali, Viral and nonviral delivery systems for gene delivery, Adv. Biomed. Res. 1 (2012) 27.
[53] S.S. Minami, B. Sun, K. Popat, T. Kauppinen, M. Pleiss, Y. Zhou, M.E. Ward, P. Floreancig, L. Mucke, T. Desai, L. Gan, Selective targeting of microglia by quantum dots, J. Neuroinflammation 9 (2012) 22.